Optical bistability of metal-coated semiconductor nanocrystals

1997 J. Phys.: Condens. Matter 9 4669

(http://iopscience.iop.org/0953-8984/9/22/019)

J. Phys.: Condens. Matter **9** (1997) 4669–4680. Printed in the UK PII: S0953-8984(97)77885-8

Optical bistability of metal-coated semiconductor nanocrystals

K P Yuen and K W Yu

Department of Physics, The Chinese University of Hong Kong, Shatin, New Territories, Hong Kong

Received 17 September 1996, in final form 20 December 1996

Abstract. We study intrinsic optical bistability in nonlinear composites of coated spheres, motivated by a recent experiment on small-particle heterogeneous systems. A self-consistent theory is applied to calculate the local fields in composites of coated spheres with a nonlinear dielectric core and a metallic shell, embedded in a linear host. To study the resonance response, we use the spectral representation and find that the local field in the core generally consists of two resonant terms, each of which has a form similar to that in the case of spherical inclusions but with a pole whose location and residue depend strongly on the dielectric constant of the core material as well as on the thickness of the shell. Thus by tuning the relevant microstructure parameters, it may be possible to reduce the threshold applied field and enhance the bistable response. Model calculations on various physical quantities are performed in accord with the experimental conditions.

1. Introduction

With the advent of high-power coherent light sources, the physics of optical nonlinearities has become a rapidly growing field both in basic research and practical applications. Optical nonlinearities can be found in virtually all materials, but large nonlinear susceptibilities are restricted to some semiconducting materials and organic polymers, which are desirable for implementing promising applications such as optical bistability, optical phase conjugation and optical switching [1]. In particular, the optical nonlinearities of composite materials of metal and semiconductor nanocrystallites have attracted much attention [1]. It is believed that one of the keys to understanding the nonlinear optical properties is to take into account the local-field effects [2]. Strong fluctuations of local fields may result in large enhancement of optical nonlinearities in small-particle composites [3]. On the other hand, quantum confinement may be an alternative source of enhancement.

Recently, there has been a growing interest in the phenomenon of optical bistability. Intrinsic bistability in metal–dielectric composites was predicted about a decade ago [4, 5]. It was demonstrated that the local fields can be enormously enhanced near the surface-plasmon resonance. Subsequent theoretical work on the enhancement of optical nonlinearities by the combination of nonlinear materials with materials showing surface-plasmon resonances was attempted by Haus, Kalyaniwalla and co-workers [6] and more recently by Bergman and co-workers [7].

Although optical bistability can be found in almost all materials, intrinsic optical bistability was hard to observe experimentally in uncoated CdS or CdSe semiconducting nanocrystals. Ricard *et al* [8] gave an account of possible difficulties in experimental

0953-8984/97/224669+12$19.50

realizations. The present work is motivated by a recent intrinsic-optical-bistability experiment by Neuendorf, Quinten and Kreibig (NQK) [9] on small-particle heterogeneous systems, in which the bistable behaviour has been observed in nanometre-size spherical CdS particles coated with silver. It turns out that quantum confinement is not important in the experimental conditions of reference [9].

The aim of the present investigation is both general and specific. We develop a general theory for the resonance properties of composites of coated spheres, and obtain tunable conditions based on the spectral representation [10]. The general theory will then be applied to the parameters relevant to the experimental conditions. Moreover, we perform model calculations so as to derive optimal conditions for the bistable operation. In this connection, the recently developed self-consistent mean-field theory [11] for nonlinear composites will be applied. A related approach was developed earlier by Zeng *et al* [12] and by Levy and Bergman [13], albeit without self-consistency.

The paper is organized as follows. In the next section, we study the spectral representation of the local field for coated spheres. On the basis of the results, in section 3 we examine the bistable condition and hence obtain the threshold applied field for the onset of bistability. In section 4, other related physical quantities such as the extinction coefficient and the reflectance at normal incidence are also calculated.

2. Spectral representation of the local field

In the Rayleigh limit for particles that are very small compared to the wavelength of light, the quasi-static approximation [14] can be used. We consider the following displacement–field characteristic for the optical Kerr effect:

$$\boldsymbol{D} = \epsilon \boldsymbol{E} + \chi |\boldsymbol{E}|^2 \boldsymbol{E} \tag{1}$$

where the dielectric constant ϵ and nonlinear susceptibility χ take on different values in the inclusion and host regions. Consider a coated sphere with a spherical core of radius a_1 and dielectric constant ϵ_c, surrounded by a concentric spherical shell of radius $a_2 > a_1$ and dielectric constant ϵ_s, suspended in a host medium of ϵ_m, with the application of an external uniform field E_0. Without loss of generality, we let $a_2 = 1$ and $a_1 = y^{1/3} < 1$. The boundary-value problem can be solved by standard electrostatics methods, and the effective linear response can be determined. In the dilute limit, the effective linear response of a small volume fraction p of coated spheres embedded in a host medium is given by [9, 15]

$$\epsilon_e = \epsilon_m + 3p\epsilon_m \frac{(\epsilon_s - \epsilon_m)(\epsilon_c + 2\epsilon_s) + (\epsilon_c - \epsilon_s)(\epsilon_m + 2\epsilon_s)y}{(\epsilon_c + 2\epsilon_s)(\epsilon_s + 2\epsilon_m) + 2(\epsilon_c - \epsilon_s)(\epsilon_s - \epsilon_m)y}. \tag{2}$$

The local field in the core can also be obtained [9, 15]:

$$E_c = \frac{9\epsilon_m \epsilon_s E_0}{(\epsilon_c + 2\epsilon_s)(\epsilon_s + 2\epsilon_m) + 2(\epsilon_c - \epsilon_s)(\epsilon_s - \epsilon_m)y}. \tag{3}$$

To study the resonant behaviour of two-component composites, it has proved convenient to adopt the spectral representation [10]. Let $w = 1 - \epsilon_e/\epsilon_m$, $x = \epsilon_c/\epsilon_m$, $v = 1 - \epsilon_s/\epsilon_m$ and $s = 1/v$; we obtain the reduced effective response $w = P_1 + P_2 + P_3$, where P_3 is the nonresonant part which vanishes in the limit of spherical inclusions; $P_1 = F_1/(s - s_1)$ and $P_2 = F_2/(s - s_2)$ are the resonant parts. Although the spectral representation was generally valid for two-component composites, we shall show that it applies to composites of coated spheres as well. We find

$$P_3 = \frac{3py(1-x)}{2+x} \tag{4}$$

$$F_1 = \frac{p(1-y)\{(2+x)[2-(2+x)s_1]+2y(1-x)[1-(1-x)s_1]\}}{(2+x)^2(s_2-s_1)} \tag{5}$$

$$F_2 = -\frac{p(1-y)\{(2+x)[2-(2+x)s_2]+2y(1-x)[1-(1-x)s_2]\}}{(2+x)^2(s_2-s_1)}. \tag{6}$$

In equations (5) and (6), s_1 and s_2 ($s_1 < s_2$) are given by

$$s_1 = \frac{8+x-2y(1-x)-\sqrt{(4-x)^2+4y(4+13x+x^2)+4y^2(1-x)^2}}{6(2+x)} \tag{7}$$

$$s_2 = \frac{8+x-2y(1-x)+\sqrt{(4-x)^2+4y(4+13x+x^2)+4y^2(1-x)^2}}{6(2+x)}. \tag{8}$$

Clearly, we have successfully extended the spectral representation to composites of coated spheres. We note that the pole location (s_1 and s_2) and strength of residue (F_1 and F_2) depend strongly on the microstructure parameters $x = \epsilon_c/\epsilon_m$ and $y = V_c/V$.

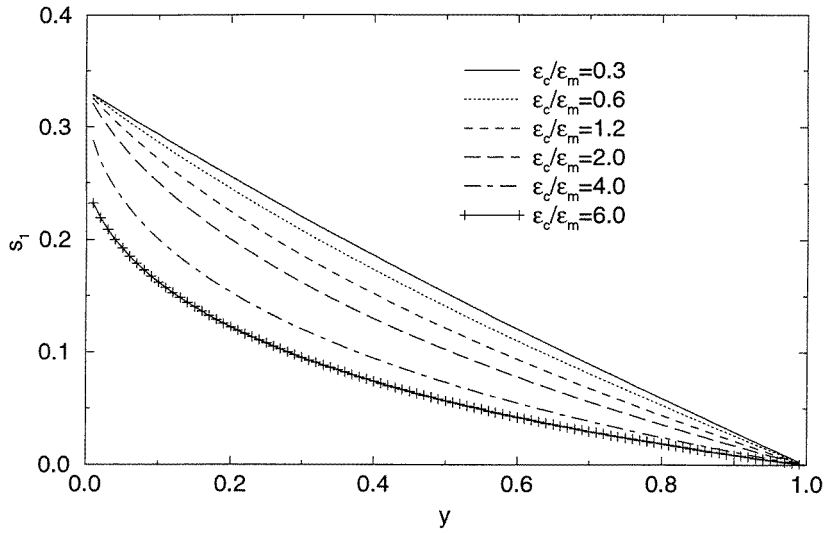

Figure 1. The pole location s_1 is plotted against the thickness parameter y for various values of ϵ_c/ϵ_m ratios. From top to bottom, $\epsilon_c/\epsilon_m = 0.3$, 0.6, 1.2, 2, 4 and 6. When we decrease y, s_1 increases towards the value at $y = 0$. In the limit of a thin shell ($y \to 1$), s_1 decreases monotonically towards zero.

In figure 1, we plot the pole location s_1 against the thickness parameter y for several values of $\epsilon_c/\epsilon_m = 0.3$, 0.6, 1.2, 2, 4 and 6. When we decrease y, s_1 increases towards the single-sphere value [10] $s_1 = 1/3$ at $y = 0$. In the limit of a thin shell ($y \to 1$), s_1 decreases monotonically towards zero. Similarly, in figure 2, we plot the pole location s_2 against y for $\epsilon_c/\epsilon_m = 0.3$, 0.6, 1.2, 2, 4 and 6. Again, when we decrease y, s_2 decreases towards the value at $y = 0$. In the thin-shell limit, s_2 increases monotonically towards unity. In figure 3, we plot the normalized residue F_1/p against y for $\epsilon_c/\epsilon_m = 0.3$, 0.6, 1.2, 2, 4 and 6. In the thin-shell limit, F_1/p decreases monotonically towards zero for various ϵ_c/ϵ_m ratios. Note the interesting change of behaviour at around $\epsilon_c/\epsilon_m = 6$ in the thick-shell limit ($y \to 0$). Similarly, in figure 4, we plot the normalized residue F_2/p against y for $\epsilon_c/\epsilon_m = 0.3$, 0.6, 1.2, 2, 4 and 6. In the thin-shell limit, F_2/p decreases monotonically towards zero for

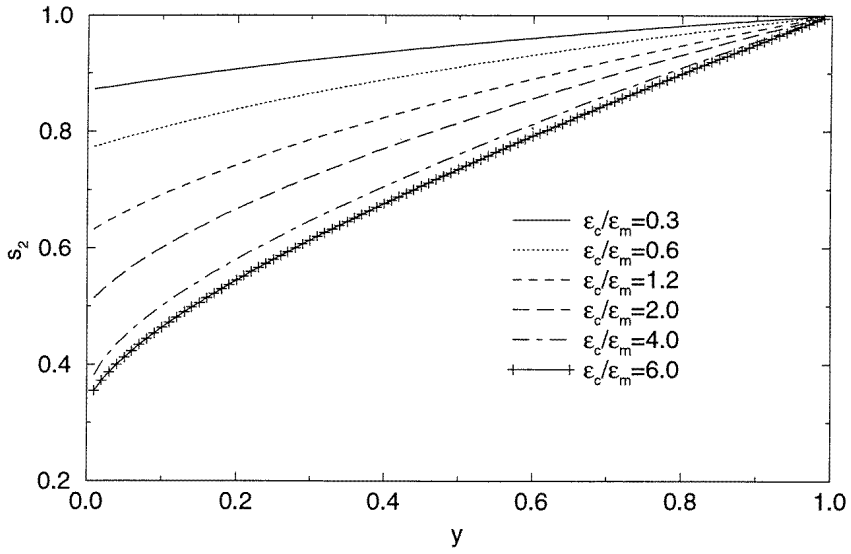

Figure 2. The pole location s_2 is plotted against the thickness parameter y for various values of ϵ_c/ϵ_m ratios as in figure 1. When we decrease y, s_2 decreases towards the value at $y = 0$. In the limit of a thin shell, s_2 increases monotonically towards unity.

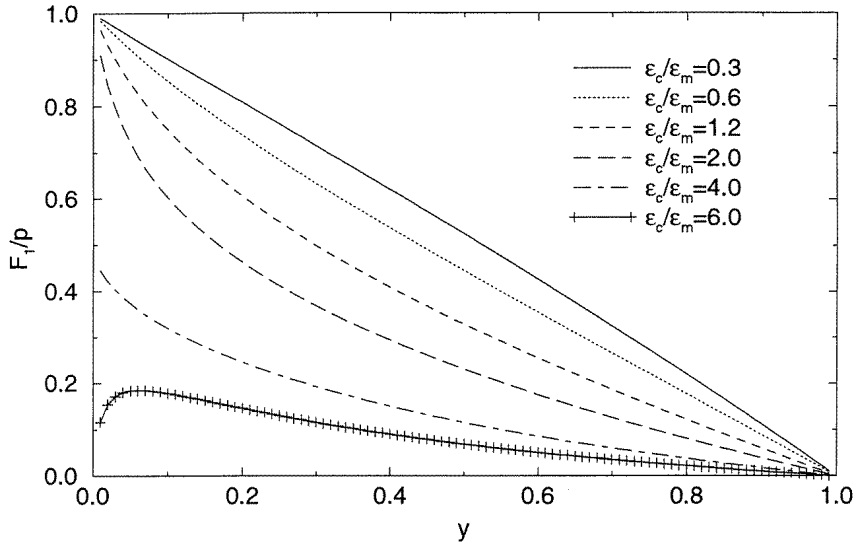

Figure 3. The normalized residue F_1/p is plotted against y for various values of ϵ_c/ϵ_m as in figure 1. In the thin-shell limit, F_1/p decreases monotonically towards zero for various ϵ_c/ϵ_m ratios. Note the change of behaviour for $\epsilon_c/\epsilon_m = 6$ in the thick-shell limit.

various ϵ_c/ϵ_m ratios. There is again a change of behaviour at around $\epsilon_c/\epsilon_m = 6$ in the thick-shell limit.

The local field E_c in the core can also be cast into a similar spectral representation:

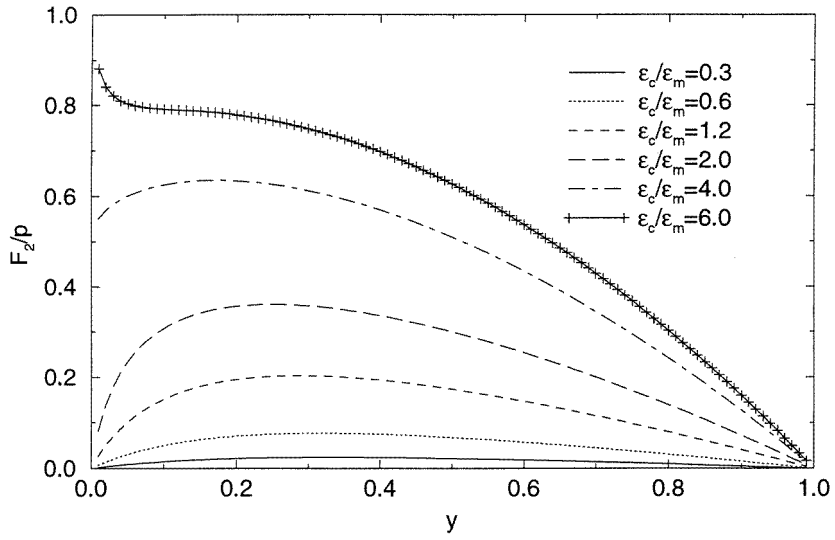

Figure 4. Similarly to in figure 3, the normalized residue F_2/p is plotted against y for various values of ϵ_c/ϵ_m as in figure 1. In the limit of a thin shell, F_2/p decreases monotonically towards zero for various ϵ_c/ϵ_m ratios. Note the change of behaviour for $\epsilon_c/\epsilon_m = 6$ in the thick-shell limit.

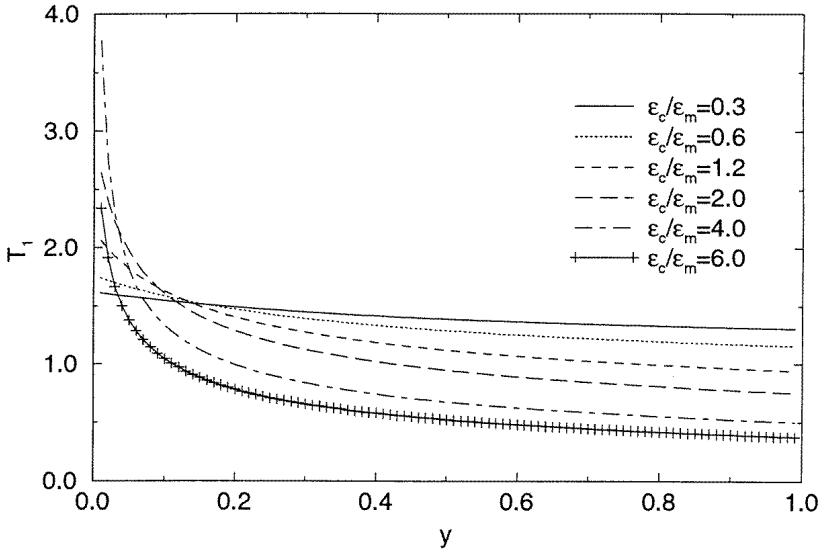

Figure 5. The residue T_1 is plotted against y for various values of ϵ_c/ϵ_m as in figure 1. T_1 decreases rapidly in the thick-shell limit and attains an asymptotic value when $y \to 1$.

$E_c = (Q_1 + Q_2)E_0$, where $Q_1 = T_1/(1 - vs_1)$ and $Q_2 = T_2/(1 - vs_2)$. We find

$$T_1 = \frac{9(1 - s_1)s_1s_2}{2(s_2 - s_1)(1 - y)} \tag{9}$$

$$T_2 = -\frac{9(1 - s_2)s_1s_2}{2(s_2 - s_1)(1 - y)}. \tag{10}$$

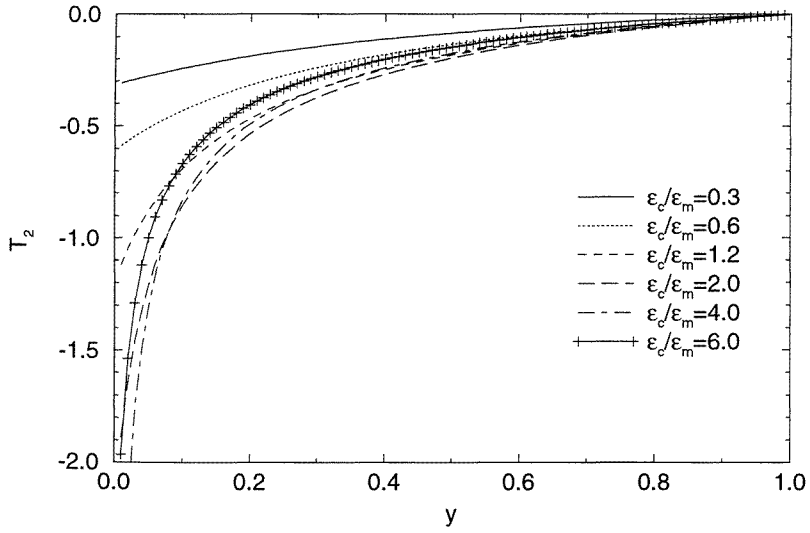

Figure 6. The residue T_2 is plotted against y for various values of ϵ_c/ϵ_m as in figure 1. T_2 increases rapidly from a negative value in the thick-shell limit and reaches zero when $y \to 1$.

We note, however, that the strength of the resonant terms depends strongly on the microstructure parameters $x = \epsilon_c/\epsilon_m$ and $y = V_c/V$. Physically T_1 is directly proportional to the strength of resonance of the optical response [9]. Clearly T_1 should be large for large resonance effects. In figure 5, we plot T_1 versus y for $\epsilon_c/\epsilon_m = 0.3$, 0.6, 1.2, 2, 4 and 6. For all ϵ_c/ϵ_m ratios, T_1 decreases monotonically with y and it attains the minimum value at $y = 1$. T_1 decreases rapidly in the thick-shell limit. In figure 6, we plot T_2 versus y for $\epsilon_c/\epsilon_m = 0.3$, 0.6, 1.2, 2, 4 and 6. The magnitude of T_2 decreases rapidly from a large value in the thick-shell limit and reaches zero when $y \to 1$.

3. The onset of bistable behaviour

Near the resonance of the first pole ($v \approx 1/s_1$), it suffices to retain only the dominant contribution Q_1:

$$E_c = \frac{T_1 E_0}{1 - v s_1} \tag{11}$$

which is of exactly the same form as that for spherical inclusions. For the present problem, the spirit of the mean-field theory [11] is to replace the dielectric constant ϵ_c by the field-dependent one $\tilde{\epsilon_c} = \epsilon_c + \chi_c |E_c|^2$ and then to perform a self-consistent evaluation of $|E_c|$. To first order, this amounts to expanding $\tilde{s_1}$ as

$$\tilde{s_1} \approx s_1 + \frac{\partial s_1}{\partial x}\, \mathrm{d}x. \tag{12}$$

Let $B = -\partial s_1/\partial x$ and $\mathrm{d}x = \chi_c |E_c|^2/\epsilon_m$; we obtain

$$E_0^2 = \left(\frac{|v|}{T_1}\right)^2 t \left[\left(\frac{B\chi_c t}{\epsilon_m} - (s_1 - s')\right)^2 + s''^2\right] \tag{13}$$

$$B = \frac{(1-y)[2y(1-x) - (4-x) + 3(2+x)(s_2 - s_1)]}{3(2+x)^3(s_2 - s_1)} \tag{14}$$

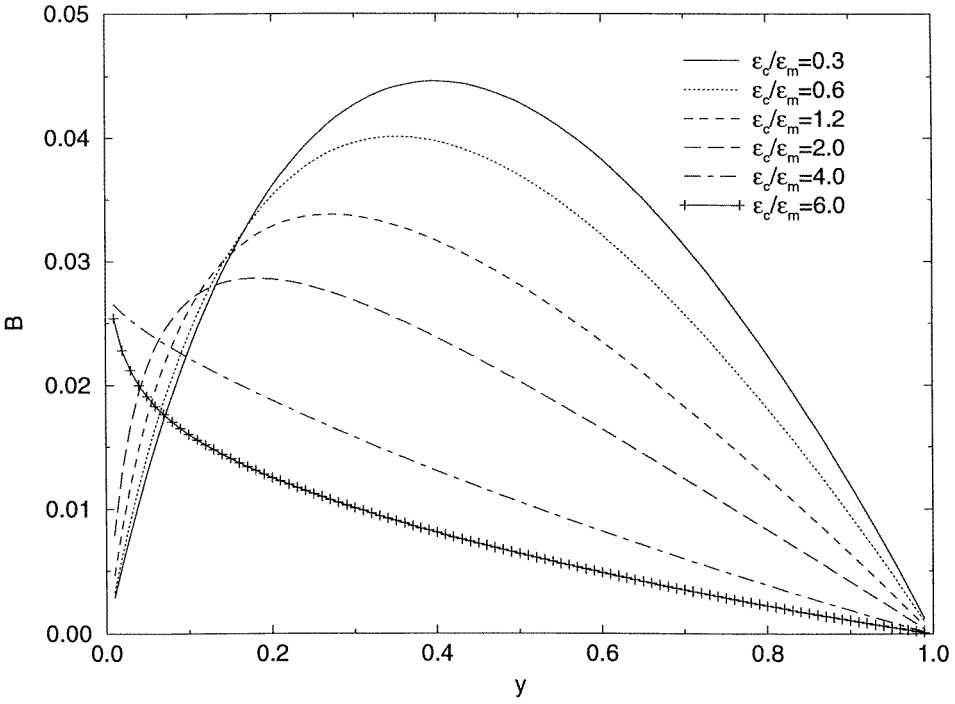

Figure 7. The factor B (defined in the text) is plotted against y for various values of ϵ_c/ϵ_m as in figure 1. For $\epsilon_c/\epsilon_m < 2$, B increases gradually in the thick-shell limit, reaches a maximum and then decreases to zero as $y \to 1$. Note the change of behaviour of B for $\epsilon_c/\epsilon_m > 2$ where B decreases monotonically towards zero as y increases.

where $t = |E_c|^2$, and s' and s'' are the real and imaginary parts of the reduced frequency $s = s' + \mathrm{i}s''$. From the experimental conditions [9], $\epsilon_s = -11.4 + 0.4\mathrm{i}$ and $\epsilon_m = 1.77$; hence $s = 0.136 + 0.004\mathrm{i}$. In figure 7, we plot the factor B against y for $\epsilon_c/\epsilon_m = 0.3$, 0.6, 1.2, 2, 4 and 6. For $\epsilon_c/\epsilon_m < 2$, B increases gradually in the thick-shell limit, reaches a maximum and then decreases to zero as $y \to 1$. Note the change of behaviour of B for $\epsilon_c/\epsilon_m > 2$ where B decreases monotonically towards zero as y increases.

Equation (13) is a cubic equation in t, which signifies bistability [4, 5]. By differentiating equation (13) with respect to t and setting it equal to zero, we obtain a quadratic equation for t:

$$3(B\chi_c)^2 t^2 - 4\epsilon_m B\chi_c(s_1 - s')t + \epsilon_m^2[(s_1 - s')^2 + s''^2] = 0 \tag{15}$$

which admits two solutions:

$$|E_c|^2_{\text{upper}} = \frac{2\epsilon_m(s_1 - s') + \epsilon_m\sqrt{(s_1 - s')^2 - 3s''^2}}{3B\chi_c} \tag{16}$$

$$|E_c|^2_{\text{lower}} = \frac{2\epsilon_m(s_1 - s') - \epsilon_m\sqrt{(s_1 - s')^2 - 3s''^2}}{3B\chi_c}. \tag{17}$$

Putting the solutions $|E_c|^2_{\text{upper}}$ and $|E_c|^2_{\text{lower}}$ into equation (13), we obtain $E^2_{0\text{upper}}$ and $E^2_{0\text{lower}}$; we then plot them in figure 8 for $s' = 0.136$, 0.1, 0.05. Clearly, maximum bistable behaviour is obtained at around $y \approx 0.1$. We have used the experimental parameters $\epsilon_c/\epsilon_m = 4.16$ and $\chi_c = 3 \times 10^{-11}$.

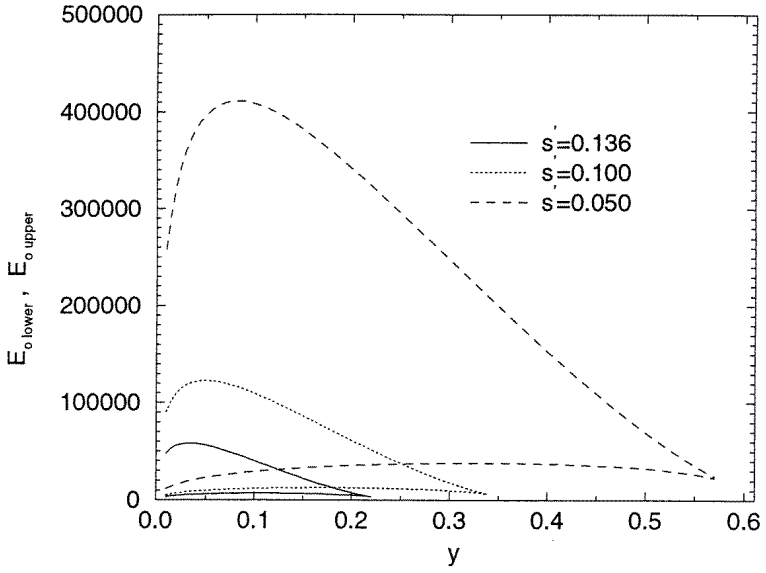

Figure 8. The lower and upper threshold fields $E_{0\text{lower}}$ and $E_{0\text{upper}}$ are plotted against y with $\epsilon_c/\epsilon_m = 4.16$, $s'' = 0.004$ and $\chi_c = 3 \times 10^{-11}$ for $s' = 0.136$, 0.1, 0.05. Maximum bistable behaviour is attained at around $y \approx 0.1$.

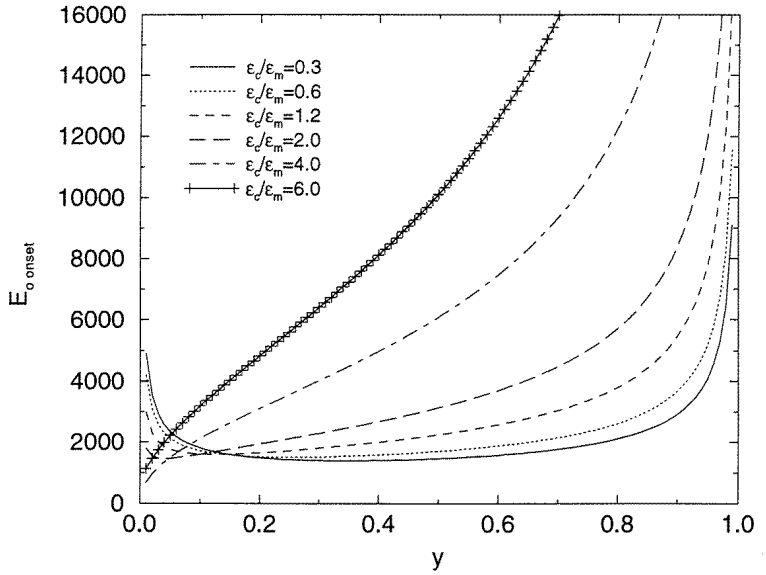

Figure 9. The onset applied field $E_{0\text{onset}}$ is plotted against y with $s' = 0.136$, $s'' = 0.004$ and $\chi_c = 3 \times 10^{-11}$ for various values of ϵ_c/ϵ_m as in figure 1. For $\epsilon_c/\epsilon_m < 2$, there exists a minimum onset field in the thick-shell region. For $\epsilon_c/\epsilon_m > 2$, $E_{0\text{onset}}$ increases monotonically as y increases.

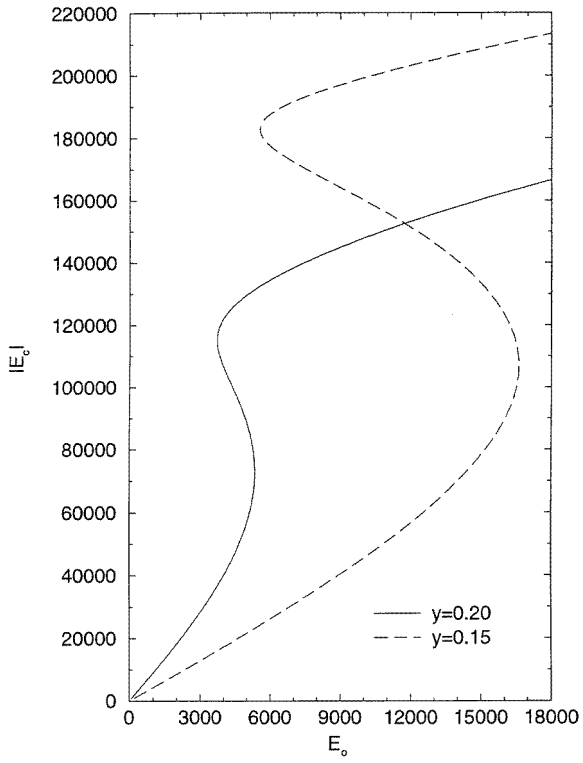

Figure 10. As a model calculation, $|E_c|$ is plotted against E_0 with $\epsilon_c/\epsilon_m = 4.16$, $\chi_c = 3\times10^{-11}$, $s' = 0.136$ and $s'' = 0.004$ for $y = 0.2$ and 0.15. The bistable behaviour is more pronounced for small y.

For the onset of bistability, we must have $|E_c|^2_{\text{upper}} = |E_c|^2_{\text{lower}}$. Equations (16) and (17) imply that

$$(s_1 - s')^2 - 3s''^2 = 0 \tag{18}$$

which admits two solutions for s':

$$s'_{\pm} = s_1 \pm \sqrt{3}s''. \tag{19}$$

For positive $|E_c|^2{}_{\text{onset}}$ and hence $E^2_{0\,\text{onset}}$, we choose s'_- and put it into equation (16) to get

$$|E_c|^2{}_{\text{onset}} = \frac{2}{\sqrt{3}}\frac{\epsilon_m s''}{B\chi_c}. \tag{20}$$

By putting equation (20) and s'_- into equation (13), we obtain

$$E^2_{0\,\text{onset}} = \frac{8}{3\sqrt{3}}\frac{\epsilon_m s''^3|v|^2}{B\chi_c T_1^2}. \tag{21}$$

In figure 9, we plot $E_{0\text{onset}}$ for $\epsilon_c/\epsilon_m = 0.3$, 0.6, 1.2, 2, 4, 6. We note that, for each value of ϵ_c/ϵ_m, $E_{0\text{onset}}$ increases rapidly in the thin-shell limit. This is attributed to the fact that B vanishes when $y \to 1$. In the thick-shell limit and when $\epsilon_c/\epsilon_m < 2$, there is also a rapid increase for $E_{0\text{onset}}$ since B vanishes in this limit. So, we find that, for $\epsilon_c/\epsilon_m < 2$, there exists a minimum onset applied field at a certain shell thickness. As is evident from

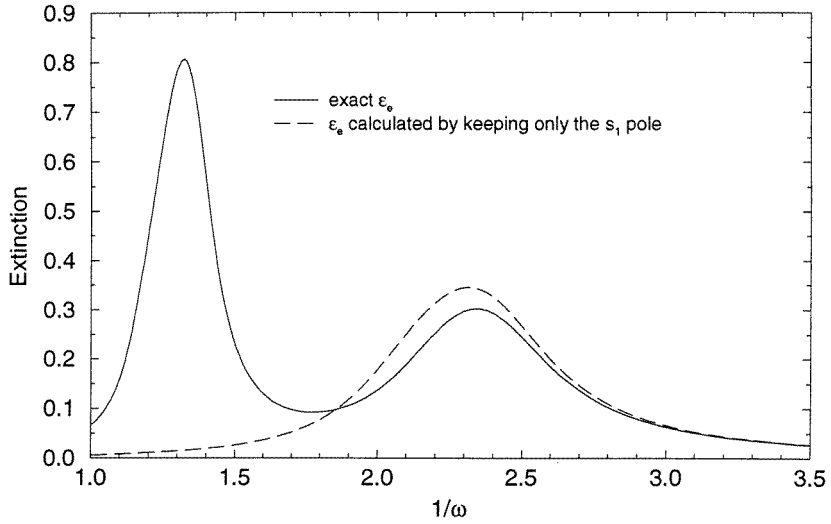

Figure 11. The extinction coefficient $\alpha(\omega)$ is plotted against the inverse frequency $(1/\omega)$ with the exact ϵ_e by retaining the full expression for the reduced response: $w = P_1 + P_2 + P_3$, and the approximate one by keeping only the first term P_1. We have assumed the Drude model for the silver coating: $\epsilon_s = 1 - \omega_p^2/\omega(\omega + \mathrm{i}\gamma)$; $\epsilon_c/\epsilon_m = 4.16$, $\omega_p = 1$, $\gamma = 0.1\omega_p$, $p = 0.3$ and $y = 0.15$. As is evident from the figure, the approximate curve has only one peak, the magnitude and position of which are close to those of the exact one. This result is expected since we have only kept the dominant pole s_1.

the figure, small onset fields can be obtained for small ϵ_c/ϵ_m ratios. This condition can be achieved by using dielectric materials with a smaller ϵ_c or a larger ϵ_m. These considerations may help to improve on the experimental conditions of NQK [9]. From figure 9, the threshold incident field can be as low as $E_0 = 2000$ V m^{-1}. The intensity I_0 is related to E_0 via $I_0 = E_0^2/\sqrt{\mu_0/\epsilon_0}$, where $\sqrt{\mu_0/\epsilon_0} = 377\ \Omega$. Hence we obtain the threshold incident intensity $I_0 = 10^4$ W m^{-2}, which is quite small. It turns out that a metallic shell can lower the threshold.

To demonstrate the bistable behaviour further, we use the experimental conditions: $\epsilon_c/\epsilon_m = 4.16$, $s' = 0.136$, $s'' = 0.004$ and $\chi_c = 3 \times 10^{-11}$, and plot the relationship between $|E_c|$ and E_0 for $y = 0.2$ and 0.15. From figure 10, bistable behaviour is more pronounced at small y.

4. The extinction coefficient and reflectance at normal incidence

Other related physical quantities can also be calculated from the spectral representation. For example, we can calculate the extinction coefficient $\alpha(\omega)$ and the reflectance R at normal incidence. Again, we retain only the dominant contribution P_1 for the reduced response w:

$$w = \frac{F_1}{s - s_1} \tag{22}$$

from which we determine the effective response

$$\epsilon_e = \left[1 + \frac{F_1(s_1 - s')}{(s' - s_1)^2 + s''^2}\right]\epsilon_m + \mathrm{i}\left[\frac{F_1 s''}{(s' - s_1)^2 + s''^2}\right]\epsilon_m. \tag{23}$$

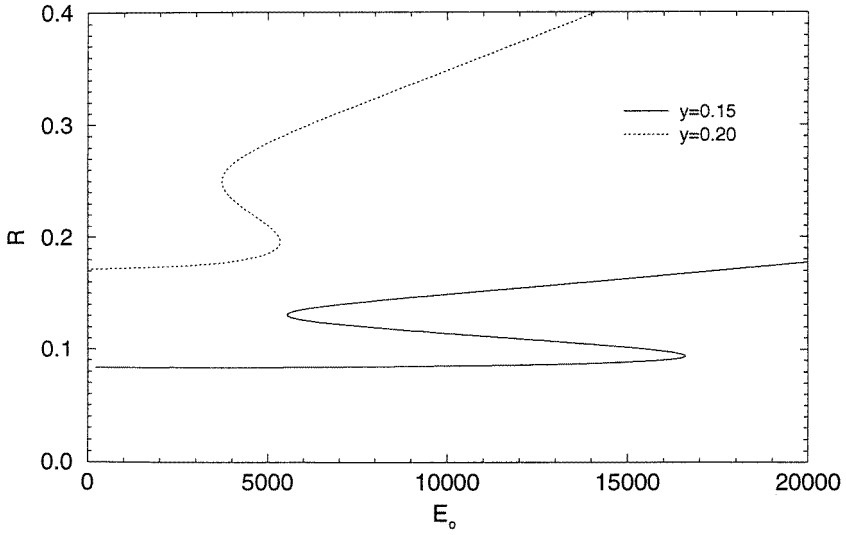

Figure 12. The reflectance $R = |(\sqrt{\epsilon_e} - 1)/(\sqrt{\epsilon_e} + 1)|^2$ is plotted against the applied field E_0 for $s = 0.136 + \mathrm{i}\,0.004$, $\epsilon_c/\epsilon_m = 4.16$, $\chi_c = 3 \times 10^{-11}$ and $p = 0.3$ for $y = 0.15$ and 0.2. Bistable behaviour is clearly observed. The hysteresis loop as formed in $y = 0.15$ is wider than that of $y = 0.2$. There is a rapid increase of the reflectance beyond the hysteresis loop for $y = 0.2$.

We write the extinction coefficient as

$$\alpha(\omega) = \omega\,\mathrm{Im}\sqrt{\epsilon_e}. \tag{24}$$

In figure 11, we plot the extinction coefficient $\alpha(\omega)$ against $1/\omega$. We have assumed the Drude model for silver coating: $\epsilon_s = 1 - \omega_p^2/\omega(\omega + \mathrm{i}\gamma)$; the parameters $\epsilon_c/\epsilon_m = 4.16$, $\omega_p = 1$, $\gamma = 0.1\omega_p$, $p = 0.3$, and $y = 0.15$ have also been used. We also plot $\alpha(\omega)$ as calculated from the full expression for ϵ_e for comparison. As is evident from the graph, the approximate $\alpha(\omega)$ has only one peak. Both its magnitude and position are close to the exact results. This result is expected since we have dropped the pole s_2 in the reduced response w. In figure 12, we plot the reflectance at normal incidence $R = |(\sqrt{\epsilon_e} - 1)/(\sqrt{\epsilon_e} + 1)|^2$ against the applied field E_0 with $s = 0.136 + \mathrm{i}\,0.004$, $\epsilon_c/\epsilon_m = 4.16$, $\chi_c = 3 \times 10^{-11}$ and $p = 0.3$ for $y = 0.15$ and 0.2. Bistable behaviour is clearly observed. The hysteresis loop as formed by $y = 0.15$ is wider than that formed by $y = 0.2$. We also note a rapid increase of the reflectance beyond the hysteresis loop for $y = 0.2$.

5. Discussion and conclusions

In this work, we study the optical bistability in a suspension of coated spheres, motivated by a recent experiment on small-particle heterogeneous systems [9]. We use the spectral representation [10] to study the resonance and bistable behaviours. We find that the strength and position of the resonance depend strongly on the dielectric constant of the core material as well as on the thickness of the shell. The theory is then applied to the experimental conditions of NQK [9] and we find that the experimental parameters are not optimal. We perform model calculations so as to suggest more favourable conditions for observing the bistability. Other related physical quantities are calculated from the spectral representation.

Here we should add a few comments on the large volume fraction $p = 0.3$ used in the model calculation of the extinction coefficient and the reflectance. The low-concentration approximation may not be accurate at such large volume fraction. Since the effective nonlinear response is proportional to the volume fraction p, if a smaller value $p = 10^{-6}$ was used in the calculations, we would find basically the same results, except that the magnitudes of the extinction coefficient and reflectance would be reduced by the corresponding small value of p used.

We hope that these analyses may ultimately help to improve the experimental conditions. In this connection, the present theory can naturally be applied to other microstructures, e.g. coated spheres with metallic cores coated with nonlinear shells. Preliminary results show that similar analyses based on the spectral representation can be used. These results, together with the enhancement of optical nonlinearities due to fractal clustering [3, 9, 16, 17] in nonlinear composites, will be reported elsewhere [18].

Acknowledgment

This work was supported by the Research Grants Council of the Hong Kong Government under Project Number CUHK 461/95P.

References

[1] Ricard D 1995 *Nonlinear Optical Materials: Principles and Applications; Proc. International Enrico Fermi School of Physics Course CXXVI* ed V DeGiorgio and C Flytzanis (Amsterdam: IOS Press) p 289
Flytzanis C, Hache F, Klein M C, Ricard D and Roussignol P 1991 *Prog. Opt.* **29** 321
[2] Keller O 1996 *Phys. Rep.* **268** 85
[3] Shalaev V M 1996 *Phys. Rep.* **272** 61
[4] Leung K M 1986 *Phys. Rev.* A **33** 2461
[5] Chemla D S and Miller D A B 1986 *Opt. Lett.* **11** 522
[6] Haus J W, Kalyaniwalla N, Inguva R and Bowden C M 1989 *J. Appl. Phys.* **65** 1420
Haus J W, Kalyaniwalla N, Inguva R, Bloemer M and Bowden C M 1989 *J. Opt. Soc. Am.* B **6** 797
Kalyaniwalla N, Haus J W, Inguva R and Birnboim M H 1990 *Phys. Rev.* A **42** 5613
[7] Bergman D J, Levy O and Stroud D 1994 *Phys. Rev.* B **49** 129
Levy-Nathansohn R and Bergman D J 1995 *J. Appl. Phys.* **77** 4263
[8] Ricard D, Ghanassi M and Schanne-Klein M C 1994 *Opt. Commun.* **108** 311
[9] Neuendorf R, Quinten M and Kreibig U 1996 *J. Chem. Phys.* **104** 6348
[10] Bergman D J 1978 *Phys. Rep.* **43** 377
[11] Yu K W, Hui P M and Lee H C 1996 *Phys. Lett.* **210A** 115
Wan W M V, Lee H C, Hui P M and Yu K W 1996 *Phys. Rev.* B **54** 3946
[12] Zeng X C, Bergman D J, Hui P M and Stroud D 1988 *Phys. Rev.* B **38** 10 970
[13] Levy O and Bergman D J 1992 *Phys. Rev.* B **46** 7189
[14] Bergman D J and Stroud D 1992 *Solid State Physics* vol 46, ed H Ehrenreich and D Turnbull (New York: Academic) p 147
[15] Yu K W, Hui P M and Stroud D 1993 *Phys. Rev.* B **47** 14 150
[16] Hui P M and Stroud D 1994 *Phys. Rev.* B **49** 11 729
Yu K W 1994 *Phys. Rev.* B **49** 9989
[17] Zhang X and Stroud D 1994 *Phys. Rev.* B **49** 944
[18] Yuen K P and Yu K W 1996 unpublished